Interactions of CCl_4 with Thin D_2O Amorphous Ice Films. 2. Variation of Desorption Kinetics with Ice Preparation Conditions and Evidence for Distinct Structures of Low-Density Amorphous Ice

V. Sadtchenko,† K. Knutsen, C. F. Giese, and W. Ronald Gentry*

Department of Chemistry, University of Minnesota, Minneapolis, Minnesota

Received: October 25, 1999; In Final Form: January 10, 2000

High sensitivity temperature-programmed desorption mass spectrometry (TPDMS) was employed in order to investigate the desorption kinetics of CCl_4 from thin (∼500 ML (ML: monolayer)) amorphous D_2O ice films. TPDMS experiments demonstrate that at low coverages CCl_4 is trapped in the pores near the surface of microscopically rough ice. Three distinct desorption features, μ-, δ-, and ϵ-CCl_4, consistent with the release of trapped CCl_4 were observed. The μ-, δ-, and ϵ-CCl_4 desorption yields demonstrate high sensitivity to the temperature and rate of ice film deposition. We interpret these results as evidence of the existence of three metastable forms of microporous amorphous ice, I_μ, I_δ, and I_ϵ. Measurements of the relative desorption yields from CCl_4 species trapped at the surface of ice films prepared at different temperatures and deposition rates were used in order to estimate the barriers to the diffusion of D_2O on the surface of I_δ ($E_{D\delta}$) and I_ϵ ($E_{D\epsilon}$). The values obtained were $E_{D\delta} = 5 \pm 1$ kcal mol^{-1} and $E_{D\epsilon} = 9 \pm 2$ kcal mol^{-1}. We suggest that I_μ, I_δ, and I_ϵ can be characterized respectively by the relative abundances of two-, three-, and four-coordinated D_2O molecules at the ice surface. A proposed phase diagram for thin D_2O ice films is presented.

Introduction

Ice is often regarded as a model system for the study of the surface properties of molecular solids. Depending on the ambient pressure and temperature, water ice can exist in a number of structurally different forms. At low pressures (<0.2 kbar), there are two known crystalline states: a diamond cubic form (I_c) and a hexagonal phase (I_h). When grown in a vacuum by vapor deposition on a cold substrate, cubic and hexagonal crystalline ice are formed at substrate temperatures above 133 and and 153 K, respectively.[1]

Deposition of water vapor at substrate temperatures below 130 K results in the formation of low-density amorphous ice ($\rho < 0.93$ g/cm^3).[1,2] Studies of the structure, morphology, surface area, density, and vapor pressure of amorphous ice films indicate a large range of physical properties, which depend on the preparation conditions.[3−21] These variations in the physical and chemical properties may be interpreted as an indication of the existence of a number of structurally different forms of amorphous ice. Laufer et al., for example, suggested that amorphous ice may exist in at least two distinct forms at $T <$ 85 K and at 85 $< T <$136.8 K, and can transform irreversibly from one form to another through a series of temperature-dependent metastable states.[11,12] Even though the variability of amorphous ice morphology has been recognized, the nature and microstructures of the various forms of amorphous ice remain unclear.

In our previous work, we employed high sensitivity TPDMS in order to investigate the adsorption of carbon tetrachloride on the surface of thin (∼ 500 ML) amorphous D_2O ice films prepared in a vacuum by D_2O vapor condensation on a cold substrate.[22] TPD spectra of CCl_4 obtained at various CCl_4 coverages, as well as isothermal studies of the carbon tetrachloride desorption kinetics, demonstrated that D_2O vapor deposition at temperatures below 130 K results in the formation of microporous amorphous ice. A typical TPD spectrum of CCl_4 from microporous amorphous D_2O ice prepared by vapor deposition at 95 K is shown in Figure 1. At low CCl_4 coverages, three distinct desorption states, labeled σ-, δ-, and ϵ-CCl_4, were observed. On the basis of extensive isothermal and TPD experiments, we demonstrated that CCl_4 adsorption on microporous ice proceeds through the formation of three-dimensional clusters in the pores of microscopically rough ice. At low coverages, CCl_4 clusters are trapped at the ice surface during TPD. Trapped CCl_4 evolves into the gas phase at two different temperatures, giving rise to the δ- and ϵ-CCl_4 desorption states. Comparison of the TPD spectra of CCl_4 from amorphous ice films deposited at several different temperatures revealed a complex dependence of δ- and ϵ-CCl_4 desorption yields on the

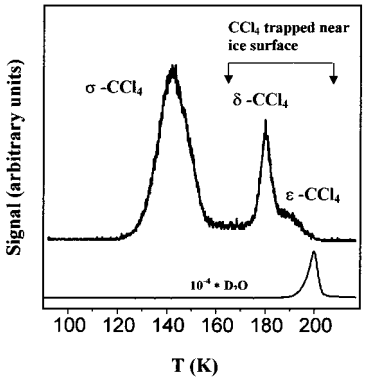

Figure 1. A typical TPD spectrum of CCl_4 from microporous amorphous ice prepared by vapor deposition at 95 K. The ice film deposition rate was 0.5 ML s^{-1}. The ice film thickness was approximately 500 ML. The D_2O TPD spectrum is shown for reference. CCl_4 coverage was approximately 0.3 ML.

* Corresponding author.
† Present address: Department of Chemistry, Indiana University, Bloomington, IN.

10.1021/jp993787s CCC: $19.00
Published on Web 05/03/2000

ice deposition conditions. These experiments clearly demonstrated that CCl_4 desorption kinetics are indeed very sensitive to the ice microstructure.

The CCl_4−ice system may seem to be intrinsically complex. Indeed, the processes which occur during simultaneous temperature-programmed desorption of trapped CCl_4 and ice are complicated and difficult to model. Fully realizing this, we do not attempt to explain in detail the kinetics of simultaneous CCl_4 and D_2O desorption. Instead, we use the TPD technique merely as a way to quantitatively determine the amount of CCl_4 trapped at the surface of microporous ice. We should emphasize that, in all experiments reported in the present paper, pure ice films first were grown under carefully controlled conditions. Only when the ice film growth was complete, and the ice film temperature was brought to a preset value of 100 K, would CCl_4 deposition commence. The primary objectives of these experiments were, first, to determine the pressures and temperatures at which the formation of pore-free ice might occur, and second, to obtain qualitative information on how the transition from microporous to pore-free ice occurs. We believe that, since the CCl_4 adsorption in our experiments takes place after the ice film deposition is complete, the comparison of CCl_4 TPD spectra from ice films grown under various conditions can provide valuable information about their respective morphologies.

Experimental Section

The experimental apparatus for TPDMS experiments has been described in detail in our previous work.[22] Only a brief account of the equipment, techniques, and procedures is given here.

The experiments were conducted in a main a vacuum chamber pumped with a 10000 L s^{-1} Varian HS-20 oil diffusion pump. D_2O ice films were vapor-deposited on a platinum substrate 5 mm in diameter and 0.5 mm thick. The substrate was in thermal contact with a liquid nitrogen cooled reservoir. A tungsten filament was positioned behind the substrate. Between 95 and 800 K, the substrate temperature was varied through a balance of radiative heating and conductive cooling.

The substrate was positioned on the line of sight of a quadrupole mass spectrometer. The detector vacuum system consisted of two differentially pumped regions. The outer region, which contained the quadrupole mass filter, ion optics, and the ion detector, was maintained at $\sim 5 \times 10^{-9}$ Torr. The inner region, which contained the electron impact ionizer, was maintained at $\sim 5 \times 10^{-10}$ Torr. Differential pumping of the detector ensured a high signal-to-background ratio. Though relatively high partial D_2O and CCl_4 pressures ($>10^{-6}$ Torr) were typically maintained inside the main chamber during the film deposition, virtually no contamination of the detector system with D_2O or CCl_4 was observed.

To avoid the mixing of the adsorbates prior to deposition, D_2O and CCl_4 were admitted into the main chamber via completely independent stainless steel lines. A direct-flow solenoid valve (General Valve), positioned at about 10 cm from the Pt substrate was used as an effusive source for D_2O deposition. The small diameter of the Pt substrate ensured the relative uniformity of the D_2O deposition flux across the substrate. The D_2O deposition flux was controlled by adjusting the stagnation pressure of the effusive source. The short actuation time of the solenoid valve (2 ms) allowed a fast cutoff of the D_2O deposition flux at the end of the deposition process.

Liquid D_2O (Isotope Laboratories) and carbon tetrachloride (Spectrum Chemicals, ACS grade) were degassed before use each day. Depending on the type of experiment (isothermal desorption or temperature-programmed desorption) the D_2O signal was monitored at *m*/*e* 22 ($D_2{}^{18}O^+$) or at *m*/*e* 20 ($D_2{}^{16}O^+$). CCl_4 was detected as *m*/*e* 117 ($C^{35}Cl_3{}^+$), the most abundant CCl_4 derived ion in the mass spectrum. CCl_4 exposures are specified in units of Torr s, the product of the time and the background pressure rise upon opening the CCl_4 doser.

A typical TPDMS experimental cycle began with cleaning of the substrate. Volatiles were removed from the substrate surface by heating of the substrate to 500 K for 20−50 s. The substrate was then rapidly cooled to the desired temperature, and a D_2O ice film was deposited. After the ice film preparation and CCl_4 dosing, a TPDMS spectrum was obtained. This experimental cycle was repeated, varying D_2O or CCl_4 conditions as desired.

Isothermal measurements of the D_2O sublimation rate at known temperatures were used in order to calibrate the mass spectrometer for desorption flux measurements. The thickness of the D_2O ice films was determined in monolayer (ML) equivalents by integration of the isothermal desorption (ID) or TPD spectra of the films over desorption time. Once the thickness of an ice film is calculated, it is possible to determine the D_2O vapor flux at the surface of the substrate during deposition. Assuming that the sticking probability for water molecules at 95−140 K is unity, the D_2O flux near the substrate surface in ML s^{-1} (ML: monolayer) units is defined as the ratio of the ice film thickness to the deposition time. These procedures provide only a rough estimate of film thickness due to uncertainties in calibration of the mass spectrometer and desorption temperature. We would like to emphasize, however, that these errors have a systematic character and allow precise relative measurements of the D_2O deposition flux in the vicinity of the substrate.

To further characterize the ice films we have investigated isothermal desorption of a multilayer CCl_4 film covered with $\sim$ 500 ML of amorphous ice.TPD spectra obtained from these experiments show that more than 95% of the carbon tetrachloride is retained until most of the overlaying D_2O ice film sublimes. These measurements clearly demonstrate that amorphous ice, though microporous, covers the substrate completely, and is free of connected pathways that traverse the entire bulk of the ice film.

TPD spectra of CCl_4 from amorphous and crystalline ice films of different thicknesses were compared in order to determine the temperature lag between heating of the Pt substrate and the ice film surface. No significant differences were observed in the TPD of CCl_4 from 500 and 1000 ML thick D_2O ice films. These results demonstrate that the temperature lag between the ice surface and the substrate is less than 1 K for ice films as thick as 500 ML.

In all experiments reported in this work, the thickness of the ice film was the same, and equal to approximately 500 ML. The partial pressure of carbon tetrachloride inside the main chamber during CCl_4 deposition was always 1×10^{-7} Torr, as measured with an ion gauge. The CCl_4 exposure was the same in all TPD experiments, and approximately equal to 3×10^{-5} Torr s. In all experiments, a 20 s delay was allowed after D_2O ice deposition before the experiment was continued with the CCl_4 deposition. This short delay ensured the cooling of the Pt substrate to 95 K whenever D_2O deposition took place at higher temperatures. A 1 s delay was also allowed before a TPDMS cycle in order to minimize the background CCl_4 signal.

Results and Analysis

TPD Spectra. Selected TPD spectra of CCl_4 from the ice films deposited at various pressures and temperatures are displayed in Figures 2−4. The D_2O deposition temperature (T_{D_2O}) and D_2O deposition flux (J_D) were varied from 95 to

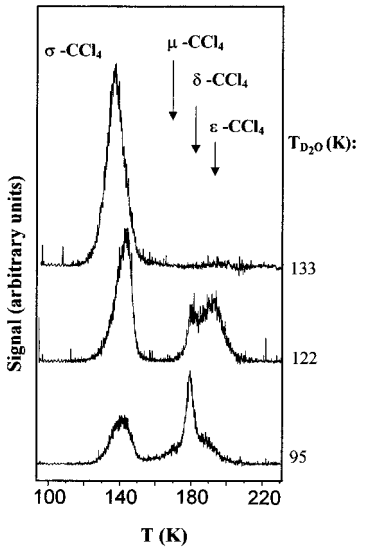

Figure 2. TPD spectra of CCl_4 from ice grown at the deposition rate $\sim$1.0 ML s^{-1}

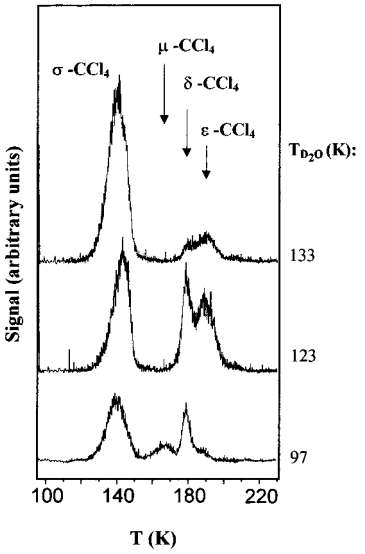

Figure 3. TPD spectra of CCl_4 from ice grown at the deposition rate $\sim$5.2 ML s^{-1}.

140 K and from 1 to 13 ML s^{-1}. As shown in Figure 5, a total of three distinct ranges of trapped CCl_4 release, labeled μ-CCl_4, δ-CCl_4, and ϵ-CCl_4 are observed in the TPD spectra.

μ-CCl_4 desorption occurs in the temperature interval from 160 to 175 K. δ-CCl_4 desorption takes place in the narrow temperature interval (>5K) around 180 K. The ϵ-CCl_4 desorption takes place at 180−200K. The desorption of μ-CCl_4 and δ-CCl_4 takes place before a significant fraction of the D_2O film has sublimed. On the other hand, the ϵ-CCl_4 desorption feature overlaps significantly with the D_2O sublimation peak. All three desorption states demonstrate a strong dependence on the D_2O deposition temperature. The μ-CCl_4 desorption state dominates the TPD spectra at low temperatures and high deposition rates, while ϵ-CCl_4 desorption is enhanced at high T_{D_2O} and low deposition rates.

The observation of the multiple desorption features in the 160−200 K temperature interval demonstrates that the release of trapped CCl_4 cannot be described simply by desorption of a multilayer D_2O/CCl_4 phase. Out of three desorption states, only the ϵ-CCl_4 desorption feature partially overlaps with the D_2O sublimation peak and may, thus, be explained by concurrent

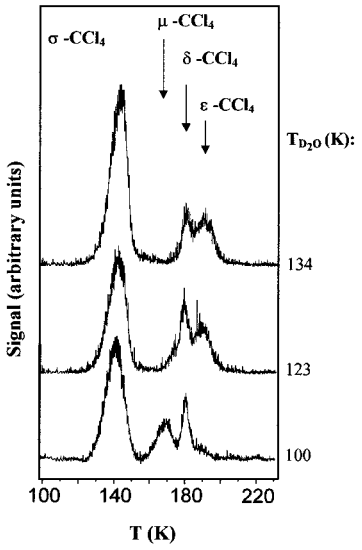

Figure 4. TPD spectra of CCl_4 from ice grown at the deposition rate $\sim$13 ML s^{-1}.

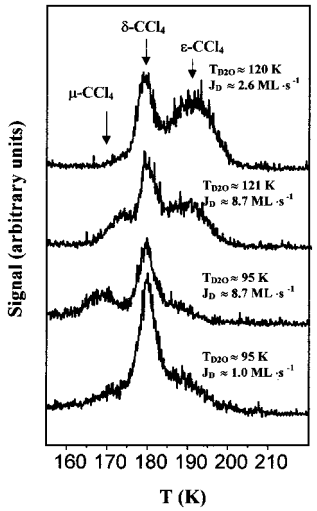

Figure 5. TPD spectra of trapped CCl_4 from ice prepared at various deposition conditions.

desorption of CCl_4 and D_2O. In our previous paper we pointed out that δ-CCl_4 desorption can be explained alternatively by (1) escape of the trapped carbon tetrachloride molecules through fractures and fissures resulting from surface and bulk restructuring during a phase transition from amorphous to hexagonal crystalline ice in the vicinity of the CCl_4 cluster or (2) decomposition of the CCl_4 clathrate.[22] Additional experiments are needed to determine precisely the mechanism of CCl_4 release. Most important, however, is the fact that the relative yields from μ-CCl_4, δ-CCl_4, and ϵ-CCl_4 demonstrate a strong dependence on the ice deposition conditions. Since carbon tetrachloride deposition takes place after the ice films have already been grown, and since the CCl_4 deposition conditions are the same for each ice film, the changes in the TPD spectra of trapped CCl_4 must reflect variations in the microstructure of the ice film with deposition conditions.

To characterize quantitatively the variations in the TPD spectra of CCl_4, we have developed a simple empirical model that describes the desorption kinetics of trapped carbon tetrachloride. The analysis of the CCl_4 TPD spectra obtained at T_{D_2O} = 95 K and characterized by low ϵ-CCl_4 yield demonstrates that the μ- and δ-CCl_4 desorption peaks can be approximated with a linear combination of two Gaussian peaks. While the

linear combination of Gaussian functions gives a satisfactory fit for the μ-CCl_4 and δ-CCl_4 desorption peaks, a more complex functional form is necessary in order to simulate ϵ-CCl_4 desorption.

A close look at the CCl_4 TPD spectra obtained at D_2O temperatures of 120−125 K, and characterized by high ϵ-CCl_4 yield, reveals the complex character of the CCl_4 desorption. The maximum of the ϵ-CCl_4 desorption peak is shifted to lower temperatures with respect to the D_2O sublimation maximum. The asymmetric ϵ-CCl_4 peak, however, partially overlaps with the D_2O sublimation peak, indicating that ϵ-CCl_4 desorption occurs simultaneously with D_2O sublimation.

The fitting function for the ϵ-CCl_4 desorption peak was constructed using the following assumptions. First, CCl_4 desorption occurs at the rate of the ice film sublimation, i.e. the escape of carbon tetrachloride trapped in the bulk of the film is impossible until the overlaying ice has sublimed. Second, at a fixed distance from the ice/vacuum interface, the CCl_4 is distributed uniformly across the plane parallel to the ice surface. In other words, $P_{CCl4}(x,y,z) = f(z)$, where $P_{CCl4}(x,y,z)$ is the density of CCl_4 in the bulk of the ice film. Third, taking into account the immiscibility of CCl_4 and ice, the diffusion of the carbon tetrachloride in the bulk of the ice film was assumed to be slow compared to the ice and CCl_4 desorption rates for temperatures below 180−200 K. The significance of such assumptions is that distribution of CCl_4 in the bulk does not change during sublimation of a CCl_4/D_2O film, i.e., $P_{CCl4}(x,y,z)$ is independent of time or temperature.

Under these assumptions, the rate expression for desorption of trapped carbon tetrachloride is

$$R(t) = n_{CCl_4}(t)\nu_0 \exp\left(\frac{-E_{D_2O}}{RT(t)}\right) \quad (1)$$

where $n_{CCl_4}(t)$ is the density of CCl_4 at the surface of the ice film, ν_0 is a zero-order preexponential factor, E_{D_2O} is the sublimation energy of the ice film, and $T(t) = T_0 + \beta$ t is the temperature of the substrate during TPD. (β is the heating rate.)

The instantaneous surface density of CCl_4 during TPD can be related to the bulk density distribution function $P_{CCl4}(x,y,z) = f(z)$ and the thickness of the ice film $h(t)$:

$$n_{CCl_4}(t) = f(h_0 - h(t)) \quad (2)$$

where h_0 is the initial thickness of the ice film.

Assuming that D_2O sublimation is not significantly affected by the presence of CCl_4 and that the density of the ice film does not vary significantly with thickness, $h(t)$ can be determined by integration of the zero-order rate expression for sublimation of the ice film:

$$h(t) = h_0 - \frac{\nu_o}{a\rho}\int_0^t \exp\left(\frac{-E_{D_2O}}{RT(t)}\right) dt \quad (3)$$

where ρ is the average number density of H_2O molecules in the bulk of the ice film, and a is the geometrical area of the ice/vacuum interface.

Following the standard treatment, the integral expression in eq 3 can be approximated, assuming that the exponent is small.[23] The expression for $h(t)$ becomes

$$h(t) = h_0 - \frac{1}{a\,\rho}\frac{\nu_o R}{\beta E_{D_2O}} T^2 \exp\left(\frac{-E_{D_2O}}{RT(t)}\right) \quad (4)$$

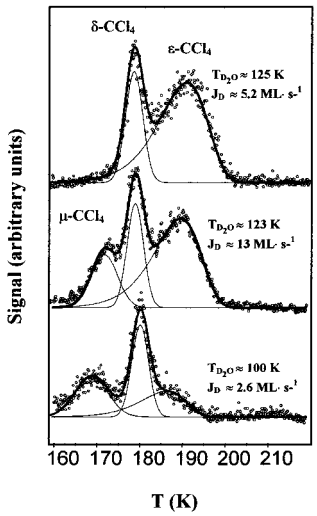

Figure 6. Typical TPD spectra of trapped CCl_4 from microporous ice and the fit.

Expression 4 allows us to derive an explicit fitting function for the ϵ-CCl_4 desorption rate if the CCl_4 distribution function $P_{CCl_4}(x,y,z) = f(z)$ is known. Several distribution functions were tried in order to fit the ϵ-CCl_4 peak using expression 1. The best results were obtained with an exponential decay of the CCl_4 density across the bulk of the ice film

$$P_{CCl_4}(x,y,z) = n_{CCl_4}(0)\exp\left(-\frac{z}{z_0}\right) \quad (5)$$

where $n_{CCl_4}(0)$ is the initial density of CCl_4 molecules at the ice surface, and z_0 is the decay constant or the penetration depth of CCl_4 in the ice film.

Several TPD spectra of CCl_4 from the ice films vapor-deposited at significantly different substrate temperatures and deposition rates, and the results of the fit, are shown in Figure 6. In the case of δ-CCl_4, the position and width of the Gaussian fit function were fixed at 180 and 5 K, respectively, while in the case of μ-CCl_4 the position and width of the Gaussian were allowed to vary. In the case of ϵ-CCl_4, the initial surface density of CCl_4 and the penetration depth z_0 were allowed to vary. The empirical model described above provides a very good fit to the experimental spectra and allows us to determine the relative yields for the three desorption states.

Discussion

Temperature Dependence. The relative variations in μ-CCl_4, δ-CCl_4, and ϵ-CCl_4 desorption yields with the temperature of D_2O deposition (yield-temperature curves) are shown in Figure 7. The D_2O flux in these experiments was approximately 2.6 ML s^{-1}. As T_{D_2O} increases, all three desorption states associated with the release of trapped CCl_4 vanish from the TPD spectra. At any deposition rate, however, the same sequence is observed: the μ-CCl_4 desorption feature declines most rapidly with the D_2O deposition temperature and disappears from the CCl_4 TPD spectra first. The δ-CCl_4 desorption yield seems to decrease less rapidly and disappears at higher temperatures compared to μ-CCl_4. The ϵ-CCl_4 feature demonstrates the most complex dependence on the D_2O deposition temperature. Low at first, the ϵ-CCl_4 yield grows with T_{D_2O}, achieving a maximum at D_2O deposition temperatures above 120−125 K, and only then declines rapidly. The strong dependence of the TPD spectra on D_2O deposition conditions implies that the structure of ice varies significantly with the temperature and rate of the ice film deposition.

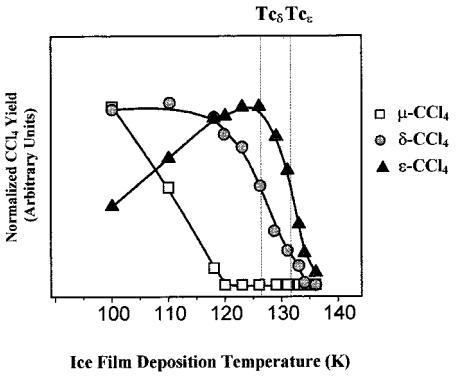

Figure 7. Dependence of μ-, δ-, and ϵ-CCl_4 yields on ice deposition temperature.

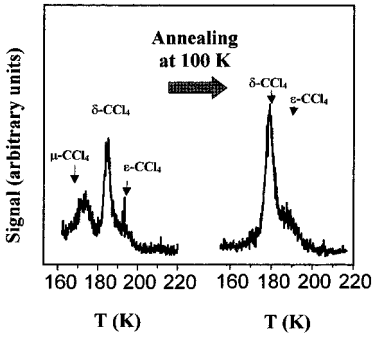

Figure 8. Effect of 30 s annealing of the ice films at 100 K on the TPD spectra of CCl_4.

The dependence of CCl_4 desorption yields on T_{D_2O} depicted in Figure 7 can be interpreted as an indication of the existence of three structurally different forms of ice capable of trapping CCl_4. It appears that these three types of ice, which we label for convenience I_μ , I_δ , and I_ϵ, may coexist in certain temperature intervals. However, at some critical temperature a transition to a more stable form takes place. As we observed repeatedly, the annealing of the ice films at 130 K for 10 −20 s leads to complete disappearance of the μ-CCl_4 desorption feature, reduction in the δ-CCl_4 yield, and an increase in the ϵ-CCl_4 desorption yield. Furthermore, the μ-CCl_4 state appears to be unstable even at 100 K. As shown in Figure 8, annealing of the ice films at 100 K for 30 s results in almost total conversion of the μ-CCl_4 state into the δ-CCl_4 state.

The TPDMS techniques applied in our experiments do not allow a direct determination of the ice film microstructure. Comparison of the TPDMS results with the data obtained from FTIR experiments, however, leads to several important conclusions. The variation with deposition temperature and pressure in the abundance of free dangling bonds (DB) in the bulk of thin H_2O ice films has been studied in detail.[8] The variation in the sum of the μ- and δ-CCl_4 yields, and the variation in the relative abundance of free dangling bonds with ice deposition temperature for the D_2O and H_2O ice films grown at approximately the same rate, are shown in Figure 9. Apparently, the decline in (μ+δ)-CCl_4 yield from D_2O ice and the decline in the absorbance by the dangling bond in the bulk of H_2O ice films occur in a similar manner and over the same range of D_2O deposition temperatures. The observation of dangling bonds in the bulk of the ice film has been associated with the presence of micropores in the ice bulk, with a large number of two- or three-coordinated water molecules at the pore surfaces.[8] The similarities in the in (μ+δ)-CCl_4 yield and DB density dependence on deposition temperature indicate that the μ- and δ-CCl_4

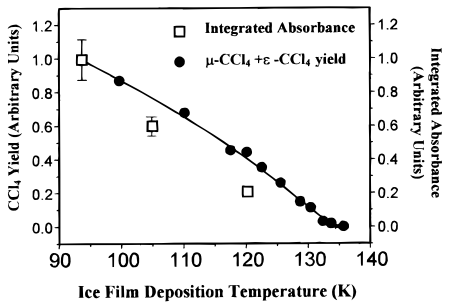

Figure 9. Dependence of combined μ- and δ-CCl_4 yield (circles), and integrated absorbance of the dangling hydrogen bond in the bulk of H_2O ice films (squares)[8] on ice deposition temperature. D_2O flux was 2.6 ML s^{-1}. Error bars represent variation of integrated absorbance with H_2O ice film thickness.

desorption states correspond to the release of CCl_4 trapped in microporous ice which is rich in incompletely coordinated D_2O molecules.

Devlin and Buch argue that, in the temperature interval from 80 to 120 K, the surface of amorphous ice consists almost exclusively of three-coordinated molecules; i.e., in this temperature range, two-coordinated molecules are mobile enough to establish fuller coordination and thus are unstable.[20] As shown in Figure 8, the rapid decline in the μ-CCl_4 yield and the increase in the δ-CCl_4 yield due to annealing at temperatures as low as 100 K indicates that the μ-CCl_4 desorption state is consistent with the release of carbon tetrachloride initially trapped in microporous ice which is rich with two-coordinated D_2O molecules.

Unlike μ-CCl_4, the δ-CCl_4 desorption state is relatively stable at temperatures below 120K. No significant changes in the CCl_4 TPD spectra were observed as a result of annealing of the ice films at 110 K for 5 min. During annealing of 200 nm thick H_2O ice films at 118 K, Zondlo et al. observed an exponential-like decay of the integrated absorbance by DB, with a time constant of $\sim$ 30 min.[8] We suggest that the δ-CCl_4 desorption state represents the release of carbon tetrachloride initially trapped in ice which is rich with three-coordinated surface D_2O molecules.

The ϵ-CCl_4 desorption feature dominates the TPD spectra at temperatures above 120 K and at low rates of an ice deposition and, therefore, is inconsistent with formation of an ice structure rich in incompletely coordinated D_2O molecules. Three-coordinated H_2O or D_2O molecules are often considered to be characteristic of the free ice surface. The decrease in the number of three-coordinated water molecules in the bulk of the ice films is interpreted as an evidence of micropore collapse and the smoothing of the ice/vacuum interface. Our observation of extensive trapping of CCl_4 at the surface and in the bulk of D_2O ice films grown at low deposition rates and at temperatures above 120 K contradicts such an interpretation of the spectroscopic data. Apparently, the decrease in the number of incompletely coordinated water molecules does not necessarily mean that the resulting ice structure is free of micropores.

This conclusion can easily be rationalized if one assumes that incompletely coordinated water molecules at the surface of the micropores are capable of establishing a fuller coordination, provided that the temperature is high enough to make them sufficiently mobile. Extensive theoretical and experimental studies conducted by Devlin and Buch provide strong evidence that, at temperatures above 120 K, the number of incompletely coordinated water molecules at the surface of amorphous and crystalline ice declines due to formation of strained hydrogen

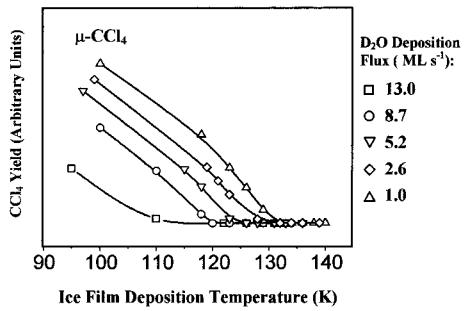

Figure 10. Dependence of μ-CCl_4 yield on ice deposition conditions.

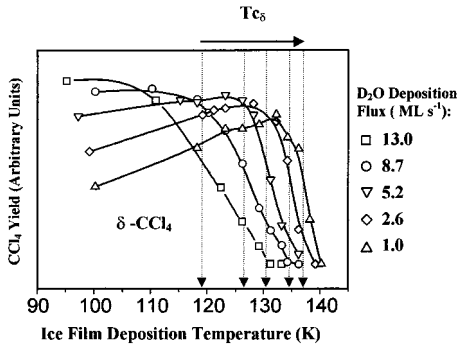

Figure 11. Dependence of δ-CCl_4 yield on ice deposition conditions.

bonds. In the case of crystalline ice this results in significant lateral disorder in the top ice bilayer.[24,25]

The increase in coordination of the D_2O molecules at the surface of the micropores must result in a reduction in their mobility relative to that of the lower-coordinated molecules, thus inhibiting the collapse of the micropores. Therefore, the micropore collapse which ultimately results in the solidification of the ice film bulk and the smoothing of the ice interface may occur at temperatures which are considerably higher than the temperature of DB absorbance decay. The microporous ice structure at this point can be viewed as an assembly of growing nanoscale clusters, with disordered four-coordinated molecules at the surface and a network of voids in between. We therefore suggest that the ϵ-CCl_4 desorption feature is consistent with the release of CCl_4 trapped in microporous ice characterized by an abundance of four-coordinated molecules at the pore surfaces.

Dependence on the Deposition Rate. Both the dependence of the CCl_4 spectra on the D_2O deposition temperature and the results of the annealing experiments demonstrate a metastable character of the μ, δ, and ϵ forms of amorphous ice. Of the three, I_ϵ is the most stable. By contrast, I_μ is is the least stable, and converts into I_δ on a time scale of seconds, even at 95 K. At D_2O deposition temperatures below a critical value T_{c_δ}, the formation of I_δ is possible, since the formation of the more stable form, I_ϵ, is kinetically inhibited at these low temperatures. At temperatures above T_{c_δ}, formation of the more stable I_μ takes place during deposition and the δ-CCl_4 yield declines rapidly. In its turn the transition from I_ϵ to polycrystalline ice (most likely to I_c) becomes possible at another critical temperature T_{c_ϵ}, and a corresponding rapid decline in the ϵ-CCl_4 yield is observed. According to Figure 7, we can define the critical temperatures approximately as those values of T_{D_2O} giving a 50% decline in the yield of the particular CCl_4 desorption feature.

Comparison of the CCl_4 yield-temperature curves obtained for different deposition rates reveal strong dependences of T_{c_δ} and T_{c_ϵ} on the D_2O deposition flux (J_d). The μ-, δ- and ϵ-CCl_4 yield-temperature curves obtained for the ice films grown at various deposition rates are shown in Figure 101−2. For δ- and ϵ-CCl_4 desorption, T_c appears to increase with the deposition flux. In the case of δ-CCl_4 desorption, T_{c_δ} changes by almost 20 K if the deposition flux is increased from 1 to 13 ML·s^{-1}. Over the same range of deposition flux, an increase of 10 K is observed for T_{c_ϵ}. In the case of μ-CCl_4 desorption, a shift in the yield curve toward higher temperatures is also apparent.

The observed dependence of the CCl_4 yield on the D_2O deposition flux indicates the importance of D_2O diffusion along the ice surface in the formation of a particular type of microporous ice. The morphology of a multilayer adsorbent is controlled by a balance between statistical roughening of the interface and surface diffusion. If diffusion is slow, the statistical fluctuation in the deposition flux and self-shadowing ultimately lead to the formation of a highly strained microporous structure.[26] To produce a smooth surface free of micropores, newly adsorbed molecules must have sufficient time to diffuse to favorable adsorption sites before being buried by the subsequent adlayer.

The average distance Λ (diffusion length) that an adsorbed molecule can travel before being buried by a subsequent adlayer can be related to the deposition flux and diffusion barrier by

$$\Lambda = A_l\left(\frac{\nu_d N}{J_d}\right)^{1/2} \exp\left(\frac{-E_{\mathrm{Diff}}}{2\,RT}\right) \tag{6}$$

where A_l is the average distance between adsorption sites, N is the density of adsorption sites, ν_d is a preexponential factor in the expression for the diffusion coefficient, E_{Diff} is a diffusion barrier, and J_d is the deposition flux.[27]

Similar to Zondlo et al. and Berland et al., we introduce a condition for the growth of pore-free, microscopically smooth ice films,[7,8] namely,

$$\Lambda(T_c) \approx A_l \tag{7}$$

As the temperature of the ice film deposition increases, the diffusion length also increases. At some critical temperature, the diffusion length becomes equal to the average distance between adsorption sites,the relaxation of the ice film interface becomes possible on the time scale of single layer deposition, and the porosity of the ice film is abruptly reduced. This sudden change in the mode of deposition is reflected in the rapid decline in the yield of the trapped CCl_4 species, since the trapping of carbon tetrachloride must occur in the ice micropores.[22]

Assuming that the rapid decline in the yield observed for δ- and ϵ-CCl_4 desorption at T_{c_δ} and T_{c_ϵ} takes place when condition 7 is satisfied, a simple expression that relates the critical temperatures to the deposition flux follows from eq 6:

$$\ln(J_d) \sim \frac{-E_{\mathrm{Diff}}}{RT_c} \tag{8}$$

According to eq 8, the dependence of the logarithm of the deposition flux on the inverse critical temperature is linear and the slope of such a plot represents the diffusion barrier for the D_2O molecules on that particular type of ice. Figure 13 demonstrates the validity of the proposed expression for the observed pressure−temperature dependence of the desorption yield, for the cases of δ- and ϵ-CCl_4 desorption. From the slope of the linear plot of $\ln(J_D)$ vs $(T_c)^{-1}$ the barriers to the diffusion of D_2O molecules on I_d (E_{d_δ}) and I_e (E_{d_ϵ}) were determined to be 5 ± 1 and 9 ± 2 kcal mol^{-1}, respectively.

Insights into the Surface Structure of Amorphous Ice. The diffusion barriers obtained from our experiments provide strong

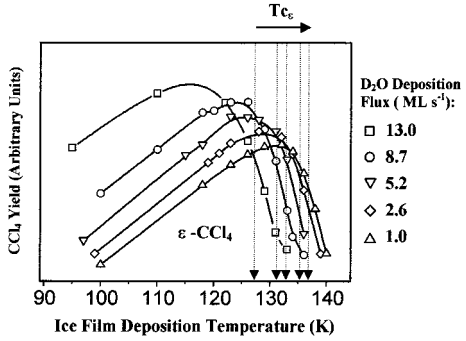

Figure 12. Dependence of ϵ-CCl_4 yield on ice deposition conditions.

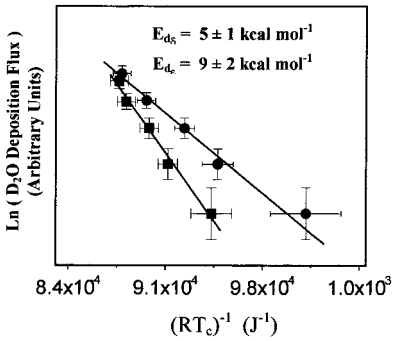

Figure 13. Plot of logarithm of the deposition flux vs critical temperature for δ-CCl_4 (circles) and ϵ-CCl_4 (squares) yields.

support for the assignment of the δ- and ϵ-CCl_4 desorption phenomena to the release of carbon tetrachloride initially trapped in ice characterized, respectively, by an abundance of three-coordinated D_2O molecules and four-coordinated D_2O molecules at the pore surfaces.

At the substrate temperatures present in our experiments, D_2O molecules impinging on the ice surface may establish three possible bonding configurations upon adsorption. At temperatures below 100 K, adsorption of D_2O molecules from the gas phase results in the formation of thermodynamically unstable two-coordinated D_2O−surface complexes having one unsaturated donor and one unsaturated acceptor site.[20] At temperatures above 100 K, the two-coordinated D_2O molecules convert into a thermodynamically more stable three-coordinated state. Such a process is likely to proceed through simple rotations of the two-coordinated D_2O molecules. Such a mechanism of transition to a three-coordinated state is expected to have a low barrier. Indeed, a very minor rearrangement of the ice surface is necessary in order to establish fuller coordination in this case.

At substrate temperatures from 100 to 120 K, the surface D_2O molecules are mostly in the three-coordinated state. Three-coordinated molecules may form strained D-bonds to the neighbor D_2O molecules, thus increasing coordination. The four-coordinated state is, of course, the most stable thermodynamically. The transition from a three-coordinated to a four-coordinated state, however, is slow at temperatures below 120K due to a large barrier. The transition to a four-coordinated state may require substantial local rearrangement of the surface D_2O molecules. Such a transition upon adsorption becomes facile only at relatively high temperatures (>120 K).

One would expect the coordination of surface D_2O molecules also to have a substantial effect on the energetics and kinetics of surface diffusion. The diffusion of $H_2O(D_2O)$ along the I_ϵ surface can be viewed as a two-step process. Assuming that most of the surface molecules of I_ϵ establish full coordination upon adsorption, a vacancy first has to be created in the top ice layer. The vacancy formation is followed by water molecule diffusion along the ice surface. In this case, the barrier to diffusion can be represented as $E_d = E_v + E_m$, the sum of the activation energy to create a vacancy in the top ice layer (E_v) and activation energy for a water monomer to migrate from one site to the next along the ice surface (E_m). The activation energy to create a vacancy in a layer of four-coordinated molecules must be close to the activation energy for formation of a vacancy in the lattice of crystalline ice. The value $E_v = (7.82 \pm 1.61)$ kcal mol^{-1} has been deduced from experimental studies of the self-diffusion mechanism of H_2O through ice.[28,29] Unfortunately, the barrier to the monomer diffusion along the surface of ice rich in four-coordinated molecules is unknown. It seems clear, however, that this activation energy should be on the order of, or less than, the barrier to diffusion along a surface rich in three-coordinated molecules. The value of the barrier to diffusion of the H_2O monomer on the ordered (rich in three-coordinated H_2O molecules) basal and prism faces of hexagonal ice $E_m = 2.5-3.0$ kcal mol^{-1} has been obtained theoretically.[30] The value of E_d thus can be estimated as $8 < E_d < 11$ kcal mol^{-1}. The value of $E_{d_\epsilon} \sim (9 \pm 2)$ kcal mol^{-1} derived from our TPDMS experiments is in excellent agreement with this estimate. The value of E_{d_ϵ} thus obtained provides strong support to the conclusion that ϵ-CCl_4 desorption originates from the release of the carbon tetrachloride initially trapped in ice films characterized by an abundance of four-coordinated D_2O molecules at the pore surfaces.

In the case of δ-CCl_4 desorption, the diffusion barrier E_{d_δ} differs from E_{d_ϵ} by approximately 5 kcal mol^{-1}. This value is on the order of the hydrogen bond energy. The difference between E_{d_δ} and E_{d_ϵ} is therefore consistent with the hypothesis that δ-CCl_4 desorption occurs as a result of the release of carbon tetrachloride initially trapped in ice pores rich with three-coordinated D_2O molecules.

On the basis of the evidence presented, we offer the following hypotheses. First, the decline in μ-CCl_4 desorption yield signifies the conversion of two-coordinated D_2O molecules into three-coordinated molecules at the ice surface. Second, the decline in δ-CCl_4 desorption yields signifies the conversion of three-coordinated D_2O molecules into four-coordinated molecules at the ice surface. Third, the decline in the ϵ-CCl_4 yield signifies the formation of pore-free, solid ice. The temperatures of the respective transitions from microporous to solid ice are consistent with the formation of cubic ice. Therefore, the final collapse of the micropores occurs only with the formation of a polycrystalline structure at the surface and in the bulk of the ice film.

As a further note, it is interesting to compare the diffusion barriers inferred from our TPD measurements to the values obtained in previous experiments. Berland et al., and later Zondlo et al., reported values of ~4 and 7 kcal mol^{-1}, respectively, for the barrier to the diffusion of H_2O molecules on the surface of amorphous ice.[7,8] The approaches undertaken in both experiments were similar to the one described in this work, in that they relied on monitoring the porosity of ice films deposited under various conditions. The experimental techniques used were quite different, however. Zondlo, et al. studied decay of the integrated absorbance by DB, while Berland et al. used measurements of the refractive indices of ice films in order to determine the ice density. The results of our experiments, which provide evidence for the existence of several structurally different forms of amorphous ice, may explain the discrepancies in the previous interpretations of diffusion data. Our experiments indicate that changes in the mechanism of surface diffusion take

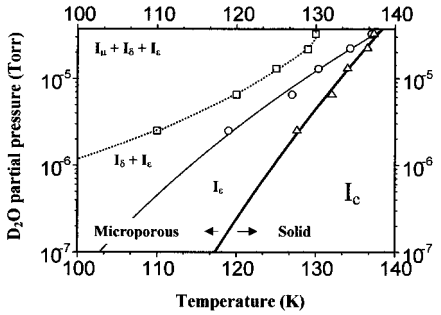

Figure 14. Tentative phase diagram of the metastable forms of amorphous D_2O ice.

place at certain temperatures of ice deposition, and that significantly different activation energies govern the diffusion of H_2O (D_2O) molecules on the surfaces of different types of ice. If our hypothesis of the existence of three distinct forms of amorphous ice is correct, the grazing angle FTIR spectroscopy experiments employed by Zondlo et al. would be sensitive only to the variation of the morphology of I_μ and I_δ,which are characterized by abundance of two- and three-coordinated water molecules, respectively. On the other hand, the refractive index measurements by Berland et al. would reflect the variations in the morphologies of all three forms of amorphous ice. The empirical models for the interpretation of the experimental results in the spectroscopic studies and ice density measurements used by Berland et al. as well as by Zondlo et al. do not include the possibility of the existence of different forms of ice. Specifically, the value of the diffusion barrier reported by Berland et al. may be interpreted as an average over the diffusion barriers of H_2O molecules on ice rich in three- and four-coordinated H_2O molecules. Similarly, the values of E_d reported by Zondlo et al. represent an average over the barrier to diffusion of H_2O on ice rich in three-coordinated water molecules, together with the barrier to transition of surface molecules from two- to three-coordinated states.

Relying on the hypotheses advanced above, we were able to construct a phase diagram that describes the D_2O ice surface microstructures, as shown in Figure 14. In this diagram, the data from our TPDMS measurements have been extrapolated to a wide range of D_2O pressures, using the parameters from the linear fits shown in Figure 13. The derived phase diagram allows the identification of the pressure−temperature regions where the deposition of D_2O vapor on the cold substrate results in an abundance of two-, three-, and four-coordinated molecules at the ice surface.

The diagram shown in Figure 14 also identifies the $P-T$ regions where the D_2O ice is microporous. Recently Kay et. al. reported the results of surface area measurements of thin ice films prepared by various techniques.[31] According to those results, pore-free H_2O ice films can be grown at temperatures as low as 50 K if a well-collimated H_2O-vapor beam at normal incidence is used for deposition. It is necessary to emphasize that the deposition technique employed in our experiments differs significantly from the molecular beam method used by Kay et al. Since in our experiments the H_2O vapor source is located relatively close to the substrate, and since the vapor source is uncollimated, the H_2O vapor flux at the substrate surface is characterized by a large variation in the incidence angle and energy of the impinging H_2O molecules. Such a regime of ice film deposition is similar to the condensation from ambient vapor. To confirm this we compared the CCl_4 TPD spectra from ice films grown at 95 K using the effusive beam source positioned near the substrate to similar spectra from ice films prepared by pressurizing the main chamber with H_2O vapor. The CCl_4 TPD spectra from the ice films prepared by the two methods were nearly identical. Thus, no disagreement exists between our results and the those of Kay et. al. Indeed, the experiments of Kay et al. also show that highly porous ice films result from deposition at low temperatures from the ambient vapor.[31]

Conclusions

The TPDMS experiments described in this work demonstrate that studies of the desorption kinetics of weakly interacting molecules from amorphous ice films can serve as unique and powerful probes of ice surface microstructure. On the basis of measurements of the desorption yields from CCl_4 molecules trapped near ice film surfaces, several important conclusions can be derived.

First, our experiments indicate that, depending on the deposition rate and temperature, D_2O molecules at the ice surface can exist in states which are primarily two-, three-, or four-coordinated. The transition from incompletely coordinated to a four-coordinated state is kinetically inhibited at temperatures below 110−120 K.

Second, when deposited from ambient vapor the ice films are likely to be microporous at any temperature and rate of deposition which are consistent with the formation of amorphous ice, i.e., amorphous ice is always microporous. Indeed, ice films grown at D_2O deposition rates in excess of 10 ML s^{-1} are capable of trapping CCl_4 even if grown at substrate temperatures as high as 140 K. At the same time, exceedingly low deposition rates are required in order to reduce the porosity of ice films when the film growth takes place at 95 K.

Third, the decline in the number of incompletely coordinated water molecules at the ice surface or in the ice bulk does not necessarily represent the collapse of the micropores. The complete disappearance of the micropores occurs only at temperatures consistent with the formation of polycrystalline cubic ice.

Fourth, the mechanisms and energetics of D_2O surface diffusion vary significantly depending with both the temperature and the detailed microstructure of the amorphous ice.

In summary, the term "amorphous" seems to be somewhat of a misnomer when applied to ice films as prepared in our experiments. Indeed, our experiments demonstrate that at least three distinct surface microstructures exist, each of which could be said to represent a separate morphology. On the basis of this evidence, it may be stated with some justification that ice films prepared under the conditions of these experiments are never completely amorphous.

References and Notes

(1) Eizenberg, D.; Kauzmann, W. *The Structure and Properties of water*; Oxford University Press: New York, 1969.
(2) Hagen, W.; Tielens, A. G. G. M.; Greenberg, J. M. *Chem. Phys.* **1981**, *56*, 367.
(3) Ghormley, J. A. *J. Chem. Phys.* **1967**, *46*, 1321.
(4) Adamson, A. W.; Dormant, L. M.; Orem, M. *J. Colloid Interface Sci.* **1967**, *25*, 206.
(5) Ocampo, J.; Klinger, J. *J. Colloid Interface Sci.* **1982**, *86*, 377.
(6) Pletzer, R.; Mayer, E. *Nature* **1986**, *319*, 298.
(7) Berland, B. S.; Brown, D. E.; Tolbert, M. A.; George, S. M. *Geophys. Res. Lett.* **1995**, *22*, 3493−3496.
(8) Zondlo, M. A.; Onasch, T. B.; Warshawsky, M. S.; Tolbert, M. A.; Mallick, G.; Arentz, P.; Robinson, M. S. *J. Phys. Chem.* **1997**, *101*, 10887.
(9) Lofgren, P.; Ahlstrom, P.; Chakarov, D. V.; Lausmaa, J.; Kasemo, B. *Surf. Sci.* **1996**, *367*, L13.
(10) Chakarov, D. V.; Osterlund, L.; Kasemo, B. *Vacuum* **1995**, *46*, 1109.

(11) Laufer, D.; Kochavi, E.; Bar-Nun, A. *Phys. Rev.* **1987**, *B 36*, 9219.
(12) Bar-Nun, A.; Owen, T. *Astrophys. Space Sci. Libr.* **1998**, *227*, 353.
(13) Zhang, Q.; Buch, V. *J. Chem. Phys.* **1990**, *92*, 1512.
(14) Zhang, Q.; Buch, V. *J. Chem. Phys.* **1990**, *92*, 5004.
(15) Buch, V.; Devlin, J. P. *J. Chem. Phys.* **1991**, *94*, 4091.
(16) Smith, R. S.; Huang, C.; Wong, E. K. L.; Kay, B. D. *Phys. Rev. Lett.* **1997**, *79*, 909.
(17) Rowland, B.; Devlin, J. P. *J. Chem. Phys.* **1991**, *94*, 812.
(18) Rowland, B.; Fisher, M.; Devlin, J. P. *J. Phys. Chem.* **1993**, *97*, 2485.
(19) Rowland, B.; Fisher, M.; Devlin, J. P. *J. Chem. Phys.* **1991**, *95*, 1378.
(20) Devlin, J. P.; Buch, V. *J. Phys. Chem.* **1995**, *99*, 16534.
(21) Schaff, J. E.; Roberts, J. T. *J. Phys. Chem.* **1996**, *100*, 14151.
(22) Sadtchenko, V.; Knutsen, K.; Giese, C. F.; Gentry, W. R. *J. Phys. Chem.* **2000**, *B104*, 2511.
(23) Redhead, P. A. *Vacuum* **1962**, *12*, 203.
(24) Delzeit, L.; Devlin, M. S.; Rowland, B.; Devlin, J. P.; Buch, J. *J. Phys. Chem.* **1996**, *100*, 10076.
(25) Buch, V.; Delzeit, L.; Blackledge, C.; Devlin, J. P *J. Phys. Chem.* **1996**, *100*, 3732.
(26) Barabasi, A. L.; Stanley, H. E. *Fractal Concepts in Surface Growth*; Cambrige University Press: Cambrige, 1995.
(27) Smith, D. L. *Thin-Film Deposition: Principles and Practice*; McGraw-Hill: New York, 1995.
(28) Eldrup, M. *J. Chem. Phys.* **1976**, *64*, 5283.
(29) Eldrup, M.; Morgensen, O. E.; Bilgram, J. H. *J. Glaciol*. **1978**, *21*, 101.
(30) Hale, B. N.; Kiefer, J.; Ward, C. A. *J. Chem. Phys.* **1981**, *75*, 1991.
(31) Stevenson, K. P.; Kimmel, G. A.; Dohnalek, Z.; Smith, R. S.; Kay B. D. *Science* **1999**, *283*, 1505.